Coagulation of monodisperse aerosol particles by isotropic turbulence

J. Chun[a] and D. L. Koch[b]
School of Chemical and Biomolecular Engineering, Cornell University, Ithaca, New York 14853-5201

(Received 10 December 2003; accepted 30 August 2004)

The rate of coagulation of initially monodisperse aerosols due to isotropic turbulence is studied with particular emphasis on the effects of noncontinuum hydrodynamics and particle inertia. The prevalence of these two factors distinguishes aerosol coagulation from the coagulation of colloidal particles. The turbulent flow seen by an interacting pair of particles is modelled as a stochastically varying flow field that is a linear function of position. This approximation is valid because the 1–10 micron diameter particles for which turbulence dominates coagulation are much smaller than the smallest eddies of a typical turbulent flow field. It is shown that the finite mean-free path of the gas enhances the rate of coagulation and leads to a finite coagulation rate even in the absence of van der Waals attractions. The coupled effects of turbulent shear and Brownian motion are treated. As in the case of laminar shear flows, it is found that Brownian motion plays an important role in the coagulation process even when the Peclet number is moderately large. It is shown that particle inertia increases the coagulation rate in two ways. First, preferential concentration increases the radial distribution function on length scales intermediate between the Kolmogorov length scale and the particle diameter. Second, the greater persistence of particles' relative motion during their local interaction leads to an increase in coagulation rate with increasing particle Stokes number. © *2005 American Institute of Physics*. [DOI: 10.1063/1.1833406]

I. INTRODUCTION

The coalescence of aerosol drops or coagulation of aerosol particles induced by turbulent flow fields plays an important role in many natural and industrial processes. For example, the size distribution of carbon black particle aggregates synthesized in an aerosol reactor depends on the turbulence level and residence time. Coagulation also affects the size distribution of air pollutants formed in flames and may influence particle-removal technologies such as cyclones and spray towers. Turbulence in clouds affects the formation of rain drops and the scavenging of pollutants by precipitation.[1] Many attempts to predict the size distribution in clouds[1–3] have used coagulation rates and collision efficiencies based on an assumption that gravity is the primary driving force. However, for drops on the order of 10 μm or smaller, turbulence can be the predominant mechanism driving coalescence.[1] To properly assess the importance of turbulent coalescence we require an accurate prediction of the rate of coagulation that takes account of the influence of particle inertia, van der Waals attractions, and noncontinuum hydrodynamic interactions between the particles.

The predominant driving force for interparticle collisions varies with the size of the particles. Typically, turbulence is the dominant driving force for particle radii of about 1 to 10 μm, while smaller particles are driven by Brownian motion and larger particles by differential sedimentation.[1] Since a typical Kolmogorov length scale η (or size of the smallest eddies) is about 1 mm in atmospheric applications and 100 μm in industrial applications, we can assume that the coagulating particles are much smaller than the length scales of the turbulent flow. As a result, the interacting particle pairs see a flow field that varies linearly with particle position with a temporally fluctuating fluid velocity gradient. By performing simulations in a model linear flow field that reproduces the flow statistics obtained from full direct-numerical simulations of turbulence, we are able to treat accurately the detailed particle–particle interactions.

Previous studies of coagulation due to turbulent shearing motions have either neglected interparticle interactions[4–7] or assumed interactions appropriate only for colloidal particles.[8] There are two important differences between the coagulation processes for aerosols and colloids. The finite mean-free path in a gas implies that noncontinuum hydrodynamic interactions occur as two aerosol particles collide. This break down of the continuum may precede or occur contemporaneously with the advance of strong van der Waals attractions. The relatively small dynamic viscosity in a gas and the large ratio of particle to gas density implies that particle inertia may influence the relative motion of aerosol particles. Thus, we will pay particular attention to the influence of noncontinuum hydrodynamics and particle inertia on the coagulation process.

We will focus on the initial stages of coagulation in monodisperse aerosols, i.e., formation of doublets from two singlets. A second-order rate expression describes this process,

$$-\frac{dn}{dt} = k_c n^2 = k_0 \alpha n^2, \tag{1}$$

where k_c is the coagulation rate coefficient and n is the bulk concentration of singlets. The coagulation rate coefficient k_c

[a]Present address: Department of Chemical Engineering, Princeton University, Princeton, New Jersey 08544.
[b]Author to whom correspondence should be adressed. Electronic mail: dlk15@cornell.edu

can be expressed as the product of an ideal rate coefficient, k_0 that ignores interparticle interactions and a collision efficiency α that accounts for the effects of interactions. In writing Eq. (1) we assume that the suspension is well mixed on a length scale larger than the Kolmogorov length scale. The time for turbulent mixing is shorter than the time over which coagulation alters the singlet concentration if the particle volume fraction is much smaller than R_λ^{-1} where R_λ is the Taylor scale Reynolds number.[9]

In most applications, aerosols have significant polydispersity. Polydispersity alters the details of the hydrodynamic and colloidal interactions that affect the collision of particles induced by the shearing motion of the turbulent gas. More importantly drops or particles with different viscous relaxation times τ_v have a relative motion induced by the turbulent acceleration of the gas.[4] Here $\tau_v = 2\rho_p a^2/9\mu$ where ρ_p is the particle density, a is the particle radius and μ is the dynamic viscosity of the fluid. By restricting our attention to initially monodisperse aerosols in the present study, we will gain an understanding of turbulent-shear-induced aerosol coagulation in the absence of the coupled driving force of turbulent acceleration. This restriction also limits the parameter space to be explored, which, as will be seen, is already quite large. This study will provide theoretical predictions for the coagulation rate in ideal laboratory experiments in which an initially monodisperse aerosol is produced by devices such as a condensation monodisperse aerosol generator.

The ideal turbulent-shear-induced coalescence rate of noninertial particles was determined by Saffman and Turner[4] under the assumption that the velocity gradient in the turbulent flow was persistent over the time scale of particle–particle encounters. The resulting ideal rate coefficient was $k_0 = 10.35\Gamma_\eta a^3$ where Γ_η is the Kolmogorov shear rate. Brunk *et al.*[8] allowed for the finite correlation time of the strain and rotation rates of the fluid and found $k_0 = 8.62(\pm 0.02)\Gamma_\eta a^3$. It will be seen below that by adopting an improved model of the turbulent velocity gradient that accounts for the log-normal distribution of the dissipation of energy in a turbulent flow, we obtain $k_0 = 8.12(\pm 0.10)\Gamma_\eta a^3$.

Brunk *et al.*[8] also considered the collision efficiency for turbulent coagulation of inertialess colloidal particles which interact solely through continuum hydrodynamic interactions and van der Waals attractions. They found that the collision efficiency α is typically 0.1 to 0.5 for colloidal systems and α decreases with increasing shear rate and particle size. This decrease in the collision efficiency can be attributed to the fact that, as the shear rate is increased, the turbulent shear is able to drive particles closer together before van der Waals forces become important. In the absence of van der Waals attractions, α would be zero.

In an aerosol system, the mean-free path of the gas λ_g (about 50 nm at standard atmospheric conditions) may be comparable with or larger than the length scale at which van der Waals attractions become important. A first attempt to characterize the effect of noncontinuum gas flow on particle interactions was undertaken by Hocking[10] who determined the lubrication forces between two particles when the gap thickness $a\varepsilon$ (ε is the nondimensional gap thickness) is much smaller than the particle radius but much larger than the mean-free path. Under these conditions, a Maxwell slip boundary condition accounts for the first noncontinuum effects. Davis[11] extrapolated this Maxwell slip result to all values of $a\varepsilon/\lambda_g$ in order to estimate the effects of noncontinuum hydrodynamic interactions on the rate of coagulation due to differential sedimentation. Subsequently Sundararajakumar and Koch[12] determined the noncontinuum lubrication force laws appropriate for order one values of $a\varepsilon/\lambda_g$ using solutions of the linearized Boltzmann equation for flow in a channel (the local geometry in a lubrication gap). In the present work, we will use Sundararajakumar and Koch results to determine the effects of finite mean-free path on the collision efficiency for turbulent coagulation.

In the absence of particle inertia, there are four parameters that affect the collision efficiency of monodisperse aerosols. The parameter $N_S = 12\pi\mu a^3\Gamma_\eta/A$ characterizes the relative strength of viscous and van der Waals forces. Here, A is the Hamaker constant. A second parameter associated with van der Waals attractions that weakly influences the collision efficiency is $N_L = 4\pi a/\xi$, where ξ is the retardation length for the van der Waals attractions. The retardation length $\xi = 100$ nm is the particle separation distance beyond which the finite propagation speed of electromagnetic waves alters the van der Waals interactions. The Knudsen number $\mathrm{Kn} = \lambda_g/a$ parametrizes the importance of noncontinuum hydrodynamic interactions. Finally, both Brownian motion and turbulent shear drive collisions of monodisperse aerosol particles, so we require a parameter indicating the strength of Brownian motion. For this purpose, we could use the ratio of convection due to shear to Brownian diffusion, i.e., the Peclet number

$$\mathrm{Pe} = \frac{\Gamma_\eta a^2}{D} = \frac{6\pi\mu a^3\Gamma_\eta}{kT}, \tag{2}$$

where D denotes the Stokes–Einstein diffusivity. Alternatively, we could use a parameter A/kT that indicates the relative strength of van der Waals and Brownian forces. Note that $\mathrm{Pe} = N_S A/(2kT)$. To understand the various physicochemical factors influencing the collision efficiency we will perform a parametric study of α as a function of N_S, Kn, and A/kT. For brevity we will only consider one value of the ratio of the particle diameter to the retardation wavelength $N_L = 238.8$ corresponding to $a = 1.9$ μm. In their study of the aggregation of colloids by turbulent shear, Brunk *et al.*[8] observed only an approximate 20% decrease in α when N_L was increased by a factor of 20. Thus, changes in the particle radius influence α primarily through their effects on Kn and N_S.

For small monodisperse particles with negligible inertia and $a \ll \eta$, the only dimensional parameter characterizing the turbulent flow that influences the coagulation rate is the Kolmogorov shear rate Γ_η. It has been shown that the two-time autocorrelations of the strain and rotation rates, which characterize the local linear flow around the interacting particle

pairs, are independent of the R_λ when all times are scaled with the inverse of the Kolmogorov shear rate.[13] Thus, our results for inertialess particles are applicable to all turbulence Reynolds numbers.

Several recent studies have considered the preferential concentration and collision rate of inertial particles in the absence of hydrodynamic and colloidal interactions. The collision rate of inertial particles in direct-numerical simulations (DNS) of isotropic turbulence is found to increase rapidly as the particle Stokes number $\mathrm{St}=\Gamma_\eta \tau_v$ is increased, reaching values that are one or two orders of magnitude larger than the inertialess result at $\mathrm{St}=O(1)$.[5,6] The collision rate is found to pass through a maximum at Stokes numbers of order one and decrease as $\mathrm{St}\to\infty$. A theoretical result for the high Stokes number limit is given by Abrahamson.[14] In typical applications where turbulent coagulation is important, the particle Stokes number is small but non-negligible. For example, water drops in air with $a=5$ μm and $\Gamma_\eta=400$ s^{-1} have $\mathrm{St}=0.12$. Because of the rapid rise in the coagulation rate at small St, it is particularly important to understand the first effects of particle inertia for $\mathrm{St}\ll 1$ and that will be the focus in our study. The time over which the relative velocities of particle pairs with $\mathrm{St}\ll 1$ remain correlated is much smaller than the time required for the particles' relative position to change by an amount comparable with the Kolmogorov scale. Thus, in the small St limit, the collisions of inertial particle pairs can be simulated using a local linear flow approximation.

A major factor contributing to the enhancement of the coagulation rate at finite St is the preferential concentration or clustering of particles due to the turbulent flow. More particles are found in regions of high strain rate than in regions of high vorticity. However, even on length scales smaller than the size of the smallest eddies or Kolmogorov length scale η, the pair probability for noninteracting, noncoalescing particles has been found to increase with decreasing radial position according to a power law,[15]

$$P(r) = n^2 g(r) = n^2 c_0 \left(\frac{\eta}{r}\right)^{c_1}, \tag{3}$$

where P is the probability of finding a pair of particles with separation r, n is the overall number density of particles, and g is the radial distribution function which would be 1 in a dilute random suspension. This power law relationship was first observed in direct-numerical simulations of Reade and Collins.[15] Subsequently, Balkovsky *et al.*[16] presented a scaling theory for the fluctuations in particle number density and the pair probability distribution function of inertial particles in turbulent flows. This theory yielded Eq. (3) along with the result that c_1 is proportional to St^2. In a study, Chun[7] analyzed the pair probability for small but nonzero Stokes number, providing a mechanistic understanding and theoretical predictions of the sub-Kolmogorov clustering that agree quantitatively with the results of full direct-numerical simulations. It was shown that the pair probability was determined by the balance of an inertially induced inward drift of the particles and turbulent relative diffusion of particle pairs. The drift was found to depend on autocorrelations and cross-correlations of the dissipation and enstrophy in the flow, which vary over the integral time scale. As a result, $c_1 = b\ \mathrm{St}^2$, where the coefficient of proportionality b depends on R_λ. Chun performed DNS to determine the statistics necessary to evaluate b for two Reynolds numbers, finding that $b=6.56$ at $R_\lambda=47.1$ and $b=7.86$ at $R_\lambda=57.3$. Falkovich and Pumir[17] also determined c_1 from direct-numerical simulations and observed that the power law exponent is approximately proportional to St^2 and grows with R_λ over the range $R_\lambda=21-310$. Falkovich and Pumir and Chun obtained similar values of c_1 for $R_\lambda=47$ and $0<\mathrm{St}<0.2$. A better understanding of the Reynolds number dependence of the clustering and coagulation of inertial particles could be obtained if the autocorrelations and cross correlations of enstrophy and dissipation are computed over a wider range of R_λ.

In a suspension of particles that coagulate or coalesce on impact and/or undergo interparticle interactions, the power law pair probability in Eq. (3) will apply for $2a\ll r\ll\eta$. A simple estimate of the increased coagulation rate due to preferential concentration would be to multiply the rate constant for inertialess particles by the pair probability [Eq. (3)] extrapolated to $r=2a$. This estimate has been suggested by Falkovich *et al.*[18]. In this paper we will test this hypothesis and determine the additional effects of inertia that occur during the local interaction of the particle pair, i.e., when $r=O(2a)$. Falkovich *et al.* suggested an additional effect of Reynolds number on the coagulation rate of inertial particles and estimated its importance using scaling arguments. Intermittency in a high Reynolds number turbulent flow implies that even when the Stokes number based on the Kolmogorov shear rate is moderately small, a small portion of the flow will have local shear rates that are large enough to lead to a Stokes number based on the local shear rate that is order one. While particles in these regions do not exhibit as large a pair distribution function, they do have large relative velocities due to their inertia and the contributions of such regions to the overall coagulation rate must be estimated separately. It should be noted however that the large value of b determined by DNS studies implies that the coagulation occurring throughout most of the flow is quite large. Thus, intermittency only becomes important at very large R_λ. Pinsky *et al.*[19] have developed a stochastic model for the strain tensor in a turbulent flow that captures the high strain rate events. This model may be useful in estimating the rate of inertia-driven coagulation of particles due to high strain rate regions of the flow. However, the model does not treat the temporal dependence of the strain rate which plays an important role in preferential concentration and coagulation in the lower strain rate regions.

The following section summarizes the simulation method, including the equations of motion for the particle pair and the method of generating the model turbulent flow field. In Sec. III, the collision efficiency of non-Brownian, inertialess particles is considered and the results including noncontinuum hydrodynamic interactions are compared with the previous work[8] on colloidal particles interacting via continuum hydrodynamic interactions. The neglect of Brownian motion and particle inertia is justified for intermediate particle radii and Kolmogorov shear rates such as $a=3$ μm and

$\Gamma_\eta = 10\ s^{-1}$. The previous study of Brunk *et al.*[8] did not consider the coupled driving forces of Brownian motion and turbulence that drive coalescence of smaller particles $a \approx 1\ \mu$m. Therefore, in Sec. IV, we consider both the ideal coagulation rate of noninteracting particles and the collision efficiency of interacting particles in the presence of Brownian motion and turbulence. In Sec. V, the coagulation rate of particles with small but nonzero Stokes numbers is considered. The results of the paper are summarized and an illustration of the dimensional results for coagulation of water droplets is presented in Sec. VI.

II. SIMULATION METHODS

To determine the coagulation rate in a homogeneous suspension in an isotropic turbulent flow, we will simulate the relative trajectory of pairs of interacting particles with separations $r < r_\infty$. We consider the trajectories of a particle labelled B relative to a particle A in a reference frame following the motion of particle A. The outer boundary, r_∞, is chosen to be much smaller than the Kolmogorov length scale η so that the fluid velocity field can be assumed to be a linear function of position for $r < r_\infty$. The turbulent velocity gradient varies stochastically with time in a manner that reproduces results for the velocity gradient obtained from direct-numerical simulations. We will use the stochastic velocity gradient models proposed by Brunk *et al.*[8] and Chun.[7] These models are described briefly in Sec. II B. The relative trajectories of the particle pairs are computed using equations of motion presented in Sec. II A. Equations are given for three different cases: (a) non-Brownian, noninertial particles, (b) Brownian particles, and (c) inertial particles.

The outer boundary should be chosen to be much larger than the particle radius to assure that particle interactions have little effect on the distribution of particle pairs outside r_∞. We typically use $r_\infty = 5a$. Brunk *et al.*[8] considered the effects of varying r_∞ and showed that this choice caused little error in the coagulation rate for non-Brownian, noninertial particles. However, the effects of finite r_∞ may be larger in the presence of Brownian motion, because the motion of Brownian particles is less persistent than that of non-Brownian particles. Thus, we will examine the effects of r_∞ on the coagulation rate of Brownian particles in Sec. IV. The clustering of inertial, non-Brownian particles, leads to a pair distribution function that varies according to Eq. (3) for length scales intermediate between $2a$ and η. We postulate that by taking proper account of this pair distribution in the region beyond r_∞, we can obtain the coagulation rate with simulation domains with modest values of r_∞/a. This postulate will be tested in Sec. V.

To generate new particle pairs in the simulation domain, we pick a point on the boundary $r = r_\infty$ at random to create a new particle B. In the simulations without Brownian motion, the initial relative velocity of the particle pair $\mathbf{U}$ is the same as that of a pair of fluid particles, i.e., $\mathbf{U} = \mathbf{r} \cdot \mathbf{\Gamma}$. Here, $\mathbf{r}$ is the position of particle B relative to particle A and $\mathbf{\Gamma}$ is the fluid velocity gradient. For Brownian particles, the initial velocity is chosen as the sum of the fluid velocity and a stochastic Brownian velocity $\mathbf{U_B}$. Following a common practice in simulation of Brownian particles,[20] we do not try to resolve the short time scale of the relaxation of the particle's velocity. Instead, the Brownian velocity remains constant for a time Δt and each Cartesian component of the Brownian velocity is chosen as a Gaussian random variable with zero mean and a variance of $2kT/6\pi\mu a \Delta t$ which produces the correct relative diffusion coefficient $2kT/6\pi\mu a$ for the pair of particles at large separations. Here k is the Boltzmann constant and T is the system temperature. The finite viscous relaxation time of the particles is not important for the range of particle sizes and gas shear rates for which both turbulent shear flow and Brownian motion influence the particle motion.[7] A particle pair can be created only if $\mathbf{U} \cdot \mathbf{n}$ is negative. Here $\mathbf{n}$ is the outward unit normal to the sphere $r = r_\infty$. To reproduce the particle flux characteristic of a pair probability that is independent of angular position, we choose to create a pair with a probability $P = |\mathbf{U} \cdot \mathbf{n}| / |\mathbf{U} \cdot \mathbf{n}|_{\max}$ where $|\mathbf{U} \cdot \mathbf{n}|_{\max}$ is an estimate of the maximum value of the normal velocity that is typically encountered. For the calculations without Brownian motion, we choose $|\mathbf{U} \cdot \mathbf{n}|_{\max} = 0.52 r_\infty \Gamma_\eta$. With this choice, 2–3% of the trials for producing a new particle pair will yield $P > 1$. For those trials, we produce one particle and choose to produce a second particle with a probability of $P - 1$. For the case with Brownian motion, we use the same procedure but with an estimated maximum normal velocity that takes account of Brownian motion as well as shear-driven particle motion, i.e., $|\mathbf{U} \cdot \mathbf{n}|_{\max} = 0.52 r_\infty \Gamma_\eta + \sqrt{2kT/6\pi\mu a \Delta t}$.

The relative trajectories of particle pairs are computed using a fifth-order Runge–Kutta algorithm with an adaptive time step and a maximum time step of $0.1 \min(\Gamma_\eta^{-1}, 6\pi\mu a^3/kT)$. Particle pairs are removed from the simulation when they come into contact and the total number of contact events R_{hit} as well as the total number of trials R_{trial} for producing pairs is recorded. Typically, we take 25 trials for making a particle at each time step so that the number of pairs in the domain at any time is approximately 2500. The simulation is run for 20 Kolmogorov times in order to achieve a statistical steady state. Thereafter, the number of particle pair collisions R_{hit} and trials for producing particle pairs R_{trial} are evaluated over a period of 930 Kolmogorov times. The resulting averages over time and particle pairs typically leads to 1.5% relative error (90% confidence intervals) in the computed coagulation rate.

In the simulations without particle inertia, the suspension can be considered homogeneous so that $P = n^2$ for $r > r_\infty$ and the assumed initial relative velocity $\mathbf{U} = \mathbf{r} \cdot \mathbf{\Gamma} + \mathbf{U_B}$ is a proper representation of the relative velocity of particle pairs at r_∞. Thus, for these cases the coagulation rate can be computed simply as the ratio of the number of particle collisions to the number of trials for making particles times the flux that would occur through the outer boundary if every trial was successful, i.e.,

$$k_c = 4\pi r_\infty^2 \frac{R_{\text{hit}}}{R_{\text{trial}}} |\mathbf{U} \cdot \mathbf{n}|_{\max}. \tag{4}$$

For particle pairs with inertia, the situation is more com-

plicated. First, it is known that the pair probability increases with decreasing radial position over a large range of separation. Our purpose here is to simulate only the small radial separations for which particle interactions and coagulation events alter the pair probability from the power law form [Eq. (3)] obtained for noninteracting *ghost* particles. Thus, instead of calculating the full rate coefficient, we will determine a factor β defined by

$$k_c = 8.12\beta\Gamma_\eta a^3 g(r=2a) \tag{5}$$

which accounts for the effects of local particle interactions on the coagulation rate constant. Here, $g(r=2a)$ is the value of the pair probability that would be obtained by extrapolating the *ghost* particle pair probability to $r=2a$. A value $\beta=1$ would correspond to the hypothetical situation in which the pair probability follows the power law form [Eq. (3)] for all separations and the rate of coagulation is equal to the inertialess result enhanced by the value of the pair probability at touching. A second complication is that the actual relative velocity of pairs of particles with finite St differs from the initial condition imposed on particle pairs at $r=r_\infty$. As a result, Chun[7] found that the power law behavior for noninteracting *ghost* particles only occurs for $r<0.8r_\infty$. If particles are generated according to a flux law based on $g=1$ and $\mathbf{U}=\mathbf{r}\cdot\mathbf{\Gamma}$ at r_∞, then the pair probability in the absence of interactions is of the power law form

$$g = c_0^{\mathrm{sim}}\left(\frac{r_\infty}{r}\right)^{c_1} \tag{6}$$

with a prefactor c_0^{sim} that can be determined from the *ghost* particle simulations of Chun.[7] Using Eq. (6) as the power law pair probability in the definition of β [Eq. (5)], we can determine β to be

$$\beta = \frac{4\pi r_\infty^2}{8.12}\frac{R_{\mathrm{hit}}}{R_{\mathrm{trial}}}|\mathbf{U}\cdot\mathbf{n}|_{\max}\frac{1}{c_0^{\mathrm{sim}}}\left(\frac{2a}{r_\infty}\right)^{c_1}. \tag{7}$$

The computed value of β can then be substituted into Eq. (5) using the power law pair probability [Eq. (3)] with a prefactor c_0 obtained from the full direct-numerical simulations of Reade and Collins[15] to obtain the predicted rate constant taking account of preferential concentration both inside and outside of r_∞.

A. Equations of motion for particle pairs

We simulate the relative trajectories of two equal-sized spheres in a linear flow field with a velocity gradient tensor $\mathbf{\Gamma}$ that fluctuates stochastically in time in such a way as to reproduce the local environment of the particle pair in an isotropic, homogeneous turbulent flow. For noninertial particles, the time evolution of the relative position $\mathbf{r}$ is given in index notation by

$$\frac{dr_i}{dt} = \Gamma_{ik}(t)r_k - C_{ij}S_{jk}r_k - \frac{2}{N_S}M_{ij}\frac{\partial\phi}{\partial r_j} + 2\sqrt{\frac{G+2H}{Pe\Delta t_f}}M_{ij}F_j^B - \frac{2}{Pe}\left[\frac{r_i}{r}\frac{dG}{dr}\right], \tag{8}$$

where lengths and times are nondimensionalized by the particle radius a and inverse Kolmogorov shear rate Γ_η^{-1}. The first term on the right-hand side of Eq. (8) is the relative velocity of two fluid particles. The second term represents the change in the particles' relative velocity due to hydrodynamic interactions. Here, $S_{jk}=\frac{1}{2}(\Gamma_{jk}+\Gamma_{kj})$ is the rate of strain tensor and C_{ij} is the hydrodynamic relative mobility tensor for two spheres in a linear shear flow. This mobility can be expressed as[21]

$$C_{ij} = A(\varepsilon)\frac{r_i r_j}{r^2} + B(\varepsilon)\left(\delta_{ij} - \frac{r_i r_j}{r^2}\right), \tag{9}$$

where $\varepsilon=(r-2a)/a$ is a normalized gap thickness. $A(\varepsilon)$ and $B(\varepsilon)$ are normalized scalar functions of relative position. Batchelor and Green[22] present tabulated results and asymptotic formulas for $A(\varepsilon)$ and $B(\varepsilon)$ for a continuum fluid.

The third term on the right-hand side of Eq. (8) is the relative motion of the pair due to van der Waals attractions. In this term, M_{ij} is the relative mobility tensor giving the relative velocity of two spheres due to equal and opposite applied forces acting on the particles. The relative mobility tensor is given by

$$M_{ij} = G(\varepsilon)\frac{r_i r_j}{r^2} + H(\varepsilon)\left(\delta_{ij} - \frac{r_i r_j}{r^2}\right), \tag{10}$$

where the scalar functions $G(\varepsilon)$ and $H(\varepsilon)$ for a continuum suspending fluid can be obtained from uniformly valid formulas provided by Jeffrey and Onishi.[23] The relative strength of viscous and van der Waals forces is characterized by a dimensionless number

$$N_S = \frac{12\pi\mu a^3\Gamma_\eta}{A} \tag{11}$$

which varies from 0.11 to 440 as the Kolmogorov shear rate is varied in the range of $\Gamma_\eta=1$ to 4000 for the water drop of $a=1.9$ μm in air. Here, A is the Hamaker constant, which has units of energy and characterizes the strength of the van der Waals attractions. The Hamaker constant depends on the nature of the aerosol material and values for several common materials are given in Russel *et al.*[24] The Hamaker constant in nonmetallic aerosols is typically $O(100\ \mathrm{kT})$ and is about a factor of 2 larger than the Hamaker constant in colloidal systems. The Hamaker constant for metallic aerosol particles is $O(10\ \mathrm{kT})$. The van der Waals attraction between two particles results from the induced-dipole/induced-dipole interactions between the molecules in the two particles. Since the induced-dipole/induced-dipole interaction can be represented in the form of a summation of characteristic electromagnetic waves, the finite propagation speed of electromagnetic waves alters these interactions on length scales comparable with the London retardation length ξ, which we take to be 100 nm.[25] Schenkel and Kitchener[25] provide an analytical approximation for the retarded van der Waals potential,

$$\phi = -\frac{1}{12(\varepsilon + 0.885N_L\varepsilon^2)} \quad \text{for} \quad \varepsilon < 4/N_L = -\left(\frac{1}{4\varepsilon}\right)\left[\frac{4.9}{15N_L\varepsilon} - \frac{8.68}{45N_L^2\varepsilon^2} + \frac{4.72}{105N_L^3\varepsilon^3}\right] \quad \text{for} \quad \varepsilon > 4/N_L, \quad \varepsilon \ll 1. \tag{12}$$

In Eq. (12), ϕ is the interparticle potential normalized by the Hamaker constant A and N_L is the diameter of the particle scaled by the London retardation wavelength, i.e., $N_L = 4\pi a/\xi$. These approximate expressions for the retarded van der Waals potential are valid in the limit of small separations (i.e., $\varepsilon \ll 1$). For $\xi \ll a$, van der Waals attractions decay in the lubrication region. This condition leads to the restriction $N_L \gg 4\pi$, which is usually satisfied when the particle radius is large enough for turbulent shear to play a role in aerosol particle coagulation. The van der Waals forces diverge at particle contact (i.e., as $\varepsilon \to 0$). To avoid numerical problems associated with this divergence, we choose $\varepsilon = 0.04\pi/N_L$ as the collision radius. van der Waals forces dominate over the shear-induced and Brownian forces at these small separations so that any particles which reach this separation will collide. Although there are technologies in which particles are purposely given opposite charges to induce coagulation, it has been argued that electrostatic particle interactions have a small effect on the coagulation rate in most natural aerosols[1] and these effects are neglected here.

The last two terms on the right-hand side of Eq. (8) give the relative displacement of the particles due to Brownian motion.[26] The relative importance of shear and Brownian motion is characterized by the Peclet number. It is interesting to note that $\mathrm{Pe} = N_S A/(2kT)$ so that the Peclet number is directly proportional to N_S for a given material and temperature. The normalized Brownian force is taken to be a Gaussian random variable which satisfies $\langle F_j^B \rangle = 0$ and $\langle F_i^B(t) F_j^B(t+\tau) \rangle = \delta_{ij}\Pi(\tau/2\Delta t_f)$ where $\Pi(x)$ is the square function which is 1 if $|x| < \frac{1}{2}$ and 0 otherwise and Δt_f is the correlation time for the Brownian force. This correlation time should be small compared with the time scales for relative motion of the particles. Typically Δt_f is set to the same value as the time step in the simulations. A relative Brownian force with zero mean acting on particles with a mobility that changes with radial separation would cause an inward drift of particle pairs toward regions of lower mobility. The final term on the right-hand side of Eq. (8) cancels this drift and assures that the equilibrium pair probability for noncoalescing particles in a dilute Brownian suspension in the absence of shear and van der Waals forces is uniform, i.e., $g(r) = 1$.

Although particles that coagulate due to turbulence typically have radii that are much larger than the mean-free path of the gas, noncontinuum effects influence the interactions between particles at small separations. The mean-free path of air at standard atmospheric conditions is about 50 nm, which is comparable with the retardation length $\xi = 100$ nm at which van der Waals forces typically become important. In a continuum fluid, the relative mobilities G and A for motion of two spheres along their line-of-centers are proportional to ε as $\varepsilon \to 0$ implying that two particles would never collide and coagulate in the absence of van der Waals attractions. A noncontinuum lubrication analysis[12] based on solutions of the linearized Boltzmann equation for channel flow yields a larger relative mobility that allows for interparticle contact. Provided that $\mathrm{Kn} = \lambda_g/a \ll 1$, noncontinuum effects only become significant when $\varepsilon = O(\mathrm{Kn}) \ll 1$. The relative mobilities in the lubrication regime can be expressed as

$$G = A = \frac{2\ \mathrm{Kn}}{f_{\mathrm{fit}}(\varepsilon/\mathrm{Kn})}, \tag{13}$$

where f_{fit}, a fit to the noncontinuum lubrication force normalized by $3\pi\mu U a^2/\lambda_g$ is given by Eq. (2.16) of Sundararajakumar and Koch.[12] A uniformly valid approximation for each of the mobilities, G and A, can be obtained by taking the sum of the noncontinuum lubrication result [Eq. (13)] and the continuum result and subtracting the continuum lubrication result $A = G = 2\varepsilon$. The tangential relative mobility functions B and H would also be modified by noncontinuum effects at small separations. Although the continuum results for B and H also vanish at small ε they go to zero very slowly (in proportion to $1/\ln \varepsilon$) and so the modification of these functions would not be expected to have a large effect on the relative trajectories of the particle pairs. Since no rigorous result is available for the tangential relative mobility when $\varepsilon = O(\mathrm{Kn})$, we use the continuum results for these mobilities.

The equations of motion for a pair of inertial particles can be written as

$$\mathrm{St}\frac{dU_i}{dt} = (A_{ij}^{11} - A_{ij}^{12})(\Gamma_{jk}(t) r_k - U_j) + \frac{2}{3}P_{ij}S_{jk}\frac{r_k}{r} - \frac{2}{N_S}\frac{\partial \phi(r)}{\partial r_i}, \tag{14}$$

$$\frac{dr_i}{dt} = U_i, \tag{15}$$

where $\mathrm{St} = m\Gamma_\eta/(6\pi\mu a)$ is the Stokes number. The hydrodynamic resistance tensors $A_{ij}^{\alpha\beta}$ giving the force on particle α due to a velocity of particle β take the form

$$A_{ij}^{\alpha\beta} = X_{\alpha\beta}(\varepsilon)\frac{r_i r_j}{r^2} + Y_{\alpha\beta}(\varepsilon)\left(\delta_{ij} - \frac{r_i r_j}{r^2}\right), \tag{16}$$

where expressions for $X_{\alpha\beta}(\varepsilon)$ and $Y_{\alpha\beta}(\varepsilon)$ in a continuum fluid are given by Jeffery and Onishi.[23] The relative resistance tensor P_{ij} can be represented by

$$P_{ij} = P_1(\varepsilon)\frac{r_i r_j}{r^2} + P_2(\varepsilon)\left(\delta_{ij} - \frac{r_i r_j}{r^2}\right), \tag{17}$$

where

$$P_1(\varepsilon) = -2(X_{11}^G(\varepsilon) - X_{12}^G(\varepsilon)),$$
$$P_2(\varepsilon) = -4(Y_{11}^G(\varepsilon) - Y_{12}^G(\varepsilon)), \tag{18}$$

and $X_{\alpha\beta}^G(\varepsilon)$ and $Y_{\alpha\beta}^G(\varepsilon)$ are scalar normal and tangential resistance functions, respectively, describing the force on particle α due to the existence of particle β in the extensional flow.[21] Only near and far field results for $X_{\alpha\beta}^G(\varepsilon)$ and $Y_{\alpha\beta}^G(\varepsilon)$ are given explicitly in Kim and Karrila,[21] but expressions valid for all ε can be obtained using the procedure described by Jeffrey and Onishi.[23]

As in the calculations without particle inertia, it is essential to modify the functions describing the hydrodynamic interactions due to normal relative motion of the particles to account for noncontinuum effects when $\varepsilon = O(\mathrm{Kn}) \ll 1$. In the lubrication regime we can relate the resistivities to the noncontinuum lubrication solution of Sundararajakumar and Koch using

$$X_{11} - X_{12} = \frac{f_{\mathrm{fit}}}{2\ \mathrm{Kn}} \tag{19}$$

and

$$P_1(\varepsilon) = -\frac{3f_{\mathrm{fit}}}{2\ \mathrm{Kn}}. \tag{20}$$

Resistance functions, $P_1(\varepsilon)$, valid for all ε can be obtained as the sum of the noncontinuum lubrication result [Eq. (20)] and the continuum result minus the continuum lubrication result.

B. Stochastic model for turbulent velocity gradient

The relative motion of two equal-sized interacting particles with radii much smaller than the Kolmogorov length scale is controlled by the local velocity gradient, $\Gamma_{ij}(t)$, of the turbulent flow. We simulate the motion of particle pairs in a linear flow field with a velocity gradient that fluctuates stochastically in time according to a model proposed by Chun.[7] This model yields probability distributions for the dissipation (magnitude of the strain rate) and enstrophy (magnitude of the rotation rate) that are log normal with variances and cross-correlations that agree with results obtained from direct-numerical simulations of isotropic turbulence. The temporal evolution of the dissipation and enstrophy in the model yields values for the autocorrelation and cross-correlation integral times that match those obtained from DNS. The strain rate and rotation rate tensors, $S_{ij} = \frac{1}{2}(\Gamma_{ij} + \Gamma_{ji})$ and $R_{ij} = \frac{1}{2}(\Gamma_{ij} - \Gamma_{ji})$, normalized by the dissipation and enstrophy are modelled as Gaussian random variables that satisfy conditions of isotropy and incompressibility. The autocorrelations of the individual components of the strain and rotation rate tensors have integral time scales that agree with those obtained from DNS. While the axes of the strain and rotation rate change over the Kolmogorov time scale, the dissipation and enstrophy (or magnitudes of strain and rotation rates) evolve more slowly on the integral time scale. Chun[7] found that accurate modelling of the two-time autocorrelations and cross-correlations of dissipation and enstrophy was essential to reproduce the preferential concentration of particle pairs in regions of high strain rate and low vorticity observed in DNS.

The model of Chun[7] more faithfully reproduces the statistics of the velocity gradient in an isotropic turbulent field than the simpler model invoked by Brunk *et al.*[8] It is therefore of interest to determine if these models yield different predictions for the ideal coagulation rate of non-Brownian, noninertial particles. Brunk *et al.* modelled the velocity gradient as a Gaussian random variable. Their model did not capture the long-time correlations of the dissipation and enstrophy. In addition, the dissipation and enstrophy in the Brunk *et al.* model have Gaussian rather than log-normal distributions. The ideal coagulation rate for noninertial, non-Brownian particles obtained from the Brunk *et al.* model is $k_0 = 8.62(\pm 0.02)\Gamma_\eta a^3$ whereas Chun's model yields $k_0 = 8.12(\pm 0.10)\Gamma_\eta a^3$ at $R_\lambda = 47.1$. Thus, the ideal coagulation rate obtained using Chun's model is 5.8% smaller. This difference can be attributed primarily to the difference between the Gaussian and log-normal distribution of the strain rate. The Kolmogorov shear rate is the root-mean-square strain rate, whereas the coagulation rate is controlled by the mean of the absolute value of the strain rate (a lower moment). The ratio of the mean of the absolute value to the root-mean-square of a log-normal variable is 4.2% smaller than the corresponding ratio for a Gaussian variable. The coagulation rate determined from our DNS of isotropic turbulence is $k_0 = 8.29(\pm 0.26)\Gamma_\eta a^3$ at $R_\lambda = 52.2$ and Wang *et al.*[27] found $k_0 = 8.31(\pm 0.17)\Gamma_\eta a^3$ from DNS at $R_\lambda = 24$. Both DNS results are in good agreement with the predictions obtained using Chun's model.

To simulate the relative trajectories of pairs of inertial particles, we need to evaluate the fluctuating velocity gradient at the center of particles. It has been recognized[5,28] that inertia causes particles whose density is greater than that of the fluid to accumulate in regions of high local strain and low vorticity. To capture this effect, we produce velocity gradient traces with values of the mean-square strain $\langle S^2 \rangle_p = \langle S_{ij} S_{ij} \rangle_p$ and mean-square rotation rate $\langle R^2 \rangle_p = \langle R_{ij} R_{ij} \rangle_p$ that match those obtained by following the trajectories of inertial particles in DNS of isotropic turbulence. The computations presented here correspond to trajectories of particles in a turbulent flow with $R_\lambda = 47.1$ and 57.3 reported by Chun.[7]

III. NON-BROWNIAN, INERTIALESS PARTICLES

In this section, we will investigate the turbulent coagulation of particles with negligible inertia and no Brownian motion. These conditions generally apply for particle radii of about $2-5\ \mu$m and moderate shear rates $\Gamma_\eta = O(10-100)\ \mathrm{s}^{-1}$. It was noted in the preceding section that the ideal coagulation rate constant in the absence of interparticle interactions was $k_0 = 8.12\Gamma_\eta a^3$. We will now consider the collision efficiency $\alpha = k_c/k_0$, the ratio of the actual rate constant to the ideal rate in the presence of hydrodynamic and/or van der Waals particles interactions.

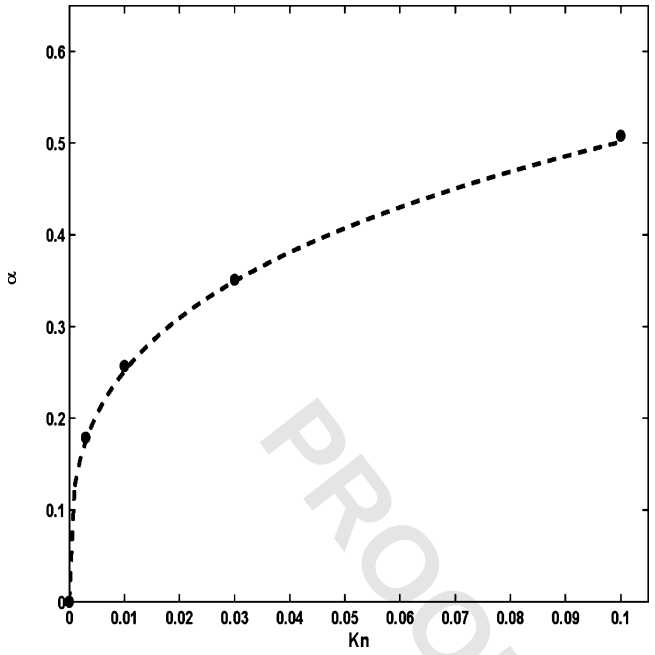

FIG. 1. The collision efficiency for particles with noncontinuum hydrodynamic interactions and no van der Waals forces is plotted as a function of the Knudsen number. The symbols are the simulation results and the 90% confidence intervals for this and all subsequent figures are smaller than the size of the symbols. The dashed line is the fit $\alpha=\mathrm{Kn}^{0.3}$.

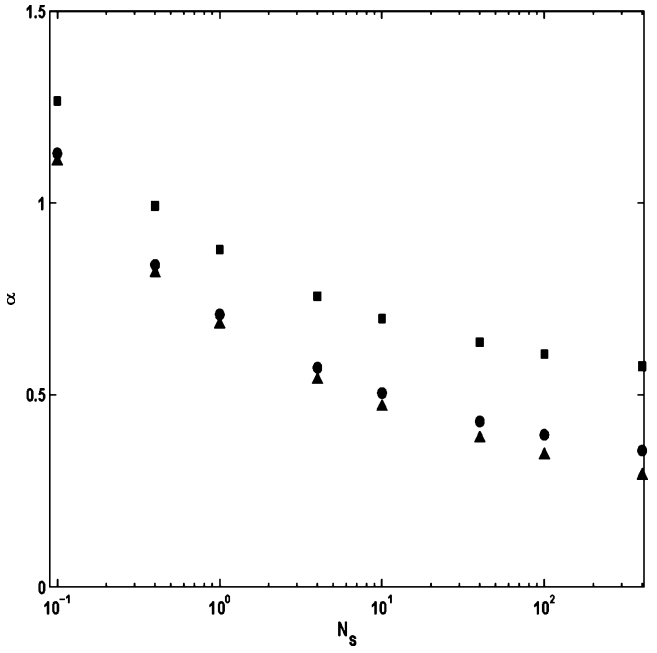

FIG. 2. The coagulation efficiency α is plotted as a function of the ratio of shear to van der Waals force, N_S, for simulations of particles with hydrodynamic and van der Waals interactions in the absence of particle inertia and Brownian motion. $N_L=238.8$, corresponding to a particle radius $a=1.9$ μm. The triangles are for continuum hydrodynamic interactions, i.e., Kn=0. The circles and squares are for noncontinuum hydrodynamic interactions with Kn=0.01 and 0.1, respectively.

We consider first a pair of particles that interact only by hydrodynamic interactions. If the suspending fluid is considered to be a continuum, no coagulation events can occur. The relative mobility for normal motion of two particles goes to zero in proportion to ε as the gap $a\varepsilon$ between the particles goes to zero. As a result, either the tangential relative motion will sweep the particles past one another or the turbulent shear will change direction and pull the particles apart before contact can occur. Noncontinuum hydrodynamic interactions lead to a larger relative mobility of particles and a finite collision efficiency, which is plotted as a function of the Knudsen number $\mathrm{Kn}=\lambda_g/a$ in Fig. 1. The results can be fit over the range of Knudsen numbers (0.005 to 0.1) explored by a power law $\alpha=\mathrm{Kn}^{0.3}$.

Next, we consider coagulation of particles experiencing van der Waals attractions and continuum hydrodynamic interactions. This situation is most relevant to colloidal particles for which the suspending medium is a liquid or to aerosol particles in high pressure gases. We will present results for a ratio of the particle diameter to the retardation wavelength, $N_L=238.8$, which corresponds to a particle radius of $a=1.9$ μm. The other parameter that governs the collision efficiency is N_S, the ratio of turbulent shear to van der Waals forces. For 1.9 μm radius water droplets in air, $N_S=0.11\Gamma_\eta$. In addition, N_S grows rapidly with particle radius $N_S\sim a^3$. Although the mobility for normal relative motion of two particles goes to zero in proportion to the separation ε, the van der Waals force diverges in proportion to ε^2 as $\epsilon\to\infty$. Thus, provided that the turbulent shear flow brings particles within a distance comparable with the retardation length $\xi=100$ nm, van der Waals forces are capable of drawing them into contact. The collision efficiency for $N_S=0.1-400$ is plotted as the triangles in Fig. 2. As N_S increases, the particles must be pushed closer together by the turbulent shear before van der Waals forces become important. For many particle pairs at high N_S, the shear changes direction or the particles are swept past each other by tangential relative motion before they can reach the very small separations where van der Waals forces would lead to coagulation. As a result, the collision efficiency decreases monotonically with N_S. The relationship $\alpha=0.76N_S^{-0.18}$ provides a good fit to the computational results throughout the range of N_S considered. It should be noted that, although the collision efficiency decreases with increasing N_S or increasing shear rate Γ_η, the overall coagulation rate coefficient increases with shear rate, i.e., $k_c\sim\Gamma_\eta^{0.82}$. In other words, the number of shear-driven pair encounters increases with increasing Γ_η, the fraction of encounters that leads to coagulation decreases, but the overall number of coagulation events increases.

Our results for the collision efficiency in continuum fluids are in good agreement with the simulations of Brunk *et al.*[8] for $N_S>10$, the parameter regime most relevant to the colloidal suspensions that were the focus of the previous study. However, the collision efficiency reported by Brunk *et al.* passed through a maximum at smaller values of N_S. It appears that this resulted from inadequate accuracy in the time integration of the pair trajectories for small N_S in the previous study. We have found that the collision efficiencies obtained with the turbulent velocity gradient models of Brunk *et al.*[8] and Chun[7] are nearly identical, despite the 5.8% difference in the ideal collision rate obtained from the two models.

van der Waals forces typically become important when the interparticle separation is comparable with the retardation length $\xi = 100$ nm. The effects of noncontinuum hydrodynamics becomes important when the particle separation is on the order of the mean free path, λ_g. At standard atmospheric conditions, $\lambda_g \approx 50$ nm. Thus, in typical aerosol applications, noncontinuum effects and van der Waals attractions are of comparable importance. Simulation results for the collision efficiency for Kn=0.01 and 0.1 are plotted in Fig. 2 as circles and squares, respectively. These Knudsen numbers correspond to 1.9 μm radius drops or particles in air at 300 K with pressures of 0.33 and 3.5 atmospheres, respectively. Noncontinuum effects increase the collision efficiency, especially at large values of N_S where the turbulent shear drives particles closer together before van der Waals forces become significant. In the limit $N_S \to \infty$, the collision efficiency for finite Kn approaches a finite value (plotted in Fig. 1) whereas the collision efficiency continues to decrease with N_S as $N_S \to \infty$ in a continuum fluid.

For parameter values typically encountered in colloidal systems, the collision efficiency ranges from 0.1 to 0.5, whereas the collision efficiency in aerosol systems is typically 0.5 to 1. The larger collision efficiency in aerosol systems results in part from the finite mean-free path of the gas. For example, at $N_S = 100$ and Kn=0.1, noncontinuum effects increase the coagulation rate by 77%. In addition, the value of N_S is typically about 100 times smaller in an aerosol than in a colloidal system for the same Kolmogorov shear rate. The smaller value of N_S results from the smaller dynamic viscosity of a gas and from the fact that the Hamaker constant is typically a factor of 2 larger in aerosols than in colloids. Since the collision efficiency increases with decreasing N_S, the smaller values of N_S in aerosol applications lead to higher collision efficiencies.

A common approximation in aerosol science is to neglect both hydrodynamic and colloidal interactions. This corresponds to an assumption that the collision efficiency is $\alpha = 1$. From the results in Fig. 2, we can see that this may typically result estimates of the coagulation rate that deviate by about a factor of 2 from the true coagulation rate.

IV. BROWNIAN PARTICLES

Particles with radii of about 0.2 to 2 μm typically coagulate due to the coupled effects of Brownian motion and turbulent shear flow. Previous theoretical studies have examined the coagulation of Brownian particles in simple shear flow.[29,30] In addition, Pnueli *et al.*[31] have performed an approximate calculation of the collection of a Brownian particle by a much larger non-Brownian particle in a persistent turbulent flow, i.e., one which does not evolve on the time scale of the particle interaction. However, we are not aware of previous theoretical studies of the coagulation of equal-sized Brownian particles in turbulent flows. Non-Brownian particles that interact purely through continuum hydrodynamic interactions can have closed orbits in a simple shear flow. Since Brownian motion or van der Waals attractions must allow pairs to move through this region of closed orbits, one may expect a particularly large role for Brownian motion in the coagulation of particles in simple shear flow. This expectation is corroborated by the perturbation analysis of Feke and Schowalter[29] for $\mathrm{Pe} \gg 1$. Although closed streamlines are absent and the velocity gradient changes with time, we will see that diffusion still influences the coagulation rate at moderate large $O(10)$ values of Pe.

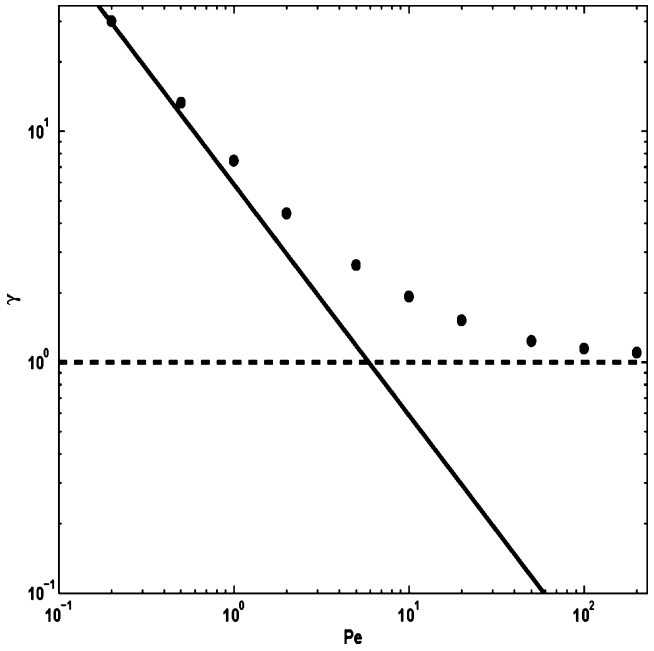

FIG. 3. The ideal coagulation rate coefficient for Brownian particles in a turbulent flow, γ, is plotted as a function of the particle Peclet number Pe. The rate coefficient is normalized by the ideal rate $8.12\Gamma_\eta a^3$ for non-Brownian particles. The circles are the simulation results. The solid and dashed lines are the ideal rates for Brownian coagulation in the absence of flow and for the turbulent coagulation of non-Brownian particles, respectively.

We consider first the ideal coalescence rate of noninteracting particles due to the coupled driving forces of turbulent shear and Brownian motion. We define γ as the ratio of this ideal rate coefficient for coupled driving forces to the ideal rate coefficient $8.12\Gamma_\eta a^3$ for turbulent shear alone. As $\mathrm{Pe} \to 0$, the ideal rate constant approaches the value $8kT/3\mu$ for Brownian coagulation[32] and so $\gamma \to 16\pi/8.12$ Pe.

Because Brownian motion is less persistent than turbulence, the influence of the outer boundary of the simulation cell is larger in the simulations with Brownian motion. An analytical solution for the case of pure Brownian motion indicates that the error due to a finite value of r_∞ is proportional to $2a/r_\infty$. By varying the value of r_∞, however, we found that the size of the simulation cell has a small (less than 2%) influence on the computed coagulation rate for $\mathrm{Pe} \geqslant 0.2$ as long as $r_\infty > 10a$. It seems likely that the effect of the outer boundary diminishes whenever a Peclet number, $\mathrm{Pe}_\infty = \Gamma_\eta r_\infty^2/D$, based on the size of the simulation domain becomes large compared with unity. We therefore report simulation results using $r_\infty = 15a$.

Simulation results for the ideal coagulation rate normalized by the rate for non-Brownian particles (circles) are plotted as a function of the Peclet number in Fig. 3. The coagulation rate is within 12% of the pure Brownian rate for

Pe<0.5. Brownian motion remains important at moderately large Pe, increasing the coagulation rate by more than 50% at Pe$=20$ and more than 10 % at Pe$=200$. The approximate expression

$$\gamma = \frac{\mathrm{Pe}^{3/2} + 4.32\ \mathrm{Pe} + 6.19\ \mathrm{Pe}^{1/2} + 17.83}{\mathrm{Pe}^{3/2} + 2.88\ \mathrm{Pe}} \tag{21}$$

lies within 4% of the simulation values for $0.5 \leqslant \mathrm{Pe} \leqslant 200$ and approaches the correct asymptotes as Pe$\rightarrow 0$ and Pe $\rightarrow \infty$.

We consider next the effects of particle interactions on the coagulation rate driven by the coupled effects of Brownian motion and turbulence. We will characterize this effect in terms of a collision efficiency α defined as the ratio of the rate coefficient in the presence of particle interactions to the ideal rate coefficient due to the coupled driving forces that is given by Fig. 3 or Eq. (21). We will present results for particles with radii $a=1.9$ μm, so that $N_L=238.8$. The noncontinuum hydrodynamic interactions between the particles are for a Knudsen number Kn$=0.1$, which corresponds to air with a pressure of 0.33 atmospheres. The Peclet number is related to N_S, the ratio of viscous to van der Waals forces, N_S, by $\mathrm{Pe}=2N_S A/kT$. Thus, for a given aerosol material, the Peclet number is simply proportional to N_S. As N_S decreases both van der Waals and Brownian forces become more important relative to viscous forces. For most aerosol materials $A/kT=10-20$, while A/kT for metals is about 100. Thus, to show the range of possible behaviors, we present results for the collision efficiencies of water drops $A/kT=10$ (circles) and metal particles $A/kT=100$ (squares) in Fig. 4. For reference we have also shown the collision efficiency (triangles) in the absence of Brownian motion and the collision efficiencies in the absence of turbulence (dashed and dashed-dotted lines) for water and metal, respectively.

The collision efficiency without Brownian motion (triangles) decreases monitonically with increasing N_S. At larger N_S, the shear is able to push the particles closer together before van der Waals attractions become important. The larger viscous resistance in the thin lubricating gaps leads to a lower collision efficiency. However, as $N_S \rightarrow \infty$, α approaches a finite value of about 0.5 due to the break down of the continuum gas flow resistance. At large values of N_S or equivalently Pe, the collision efficiencies for water (circles) and metal (squares) aerosols are similar to those in the absence of Brownian motion. However, they exhibit maxima which occur at Pe≈ 5 for both values of A/kT. At lower values of Pe, the collision efficiency approaches the value corresponding to purely Brownian particles in the absence of turbulence. The presence of Brownian motion always lowers the collision efficiency relative to the non-Brownian result (triangles), although Brownian motion increases the overall coagulation rate, i.e., the product of α from Fig. 4 and γ from Fig. 3. In a very weak shear flow $N_S \rightarrow 0$ in the absence of Brownian motion Pe$\rightarrow \infty$, the flow leads to a very slow relative motion of particles that leaves them in the vicinity of one another for an extended time. This can allow van der Waals attractions to cause coagulation even in events that would lead to no collision between noninteracting particles.

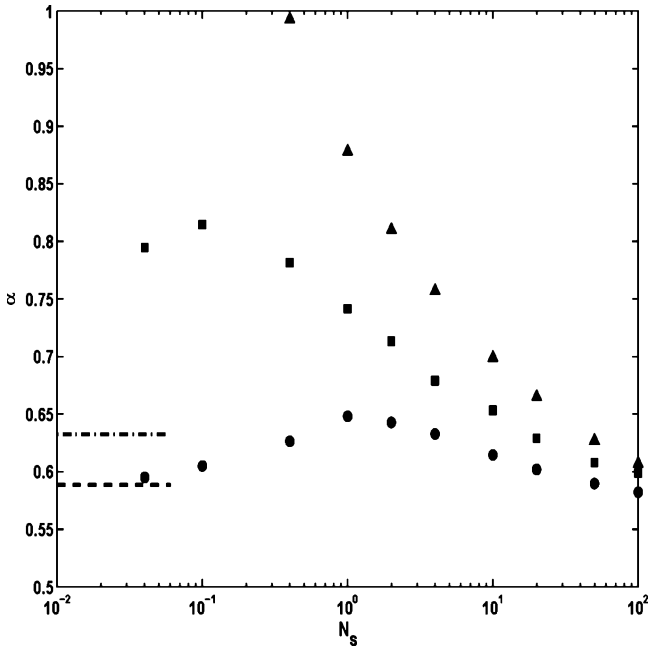

FIG. 4. The effect of Brownian motion on the collision efficiency for water drops and metal particles at room temperature. In the simulations, the particle size and Knudsen number are set to 1.9 μm and 0.1, respectively. Here α denotes the collision efficiency. The circles denote the results for water drops, i.e., $\mathrm{Pe}=5N_S$ and squares denote the results for metal particles, i.e., $\mathrm{Pe}=50N_S$. The triangles indicate the collision efficiency for non-Brownian particles, Pe$\rightarrow \infty$, and the dashed and dashed–dotted lines indicate the collision efficiencies for Brownian water ($A/kT=10$) and metal ($A/kT=100$) particles, respectively, in the absence of the turbulent flow.

This leads to an anomalously large collision efficiency $\alpha \rightarrow \infty$ as $N_S \rightarrow 0$ for Pe$=\infty$. Brownian motion limits the time of interaction and thereby mitigates the effects of van der Waals attractions at larger gap thicknesses.

V. INERTIAL PARTICLES

Particles in the size range ($a=1-10$ μm) for which turbulent shear plays an important role in driving coagulation typically have very small viscous relaxation times $\tau_v = 2\rho a^2/9\mu < 1.2\times 10^{-3}$ s. The coagulation rate of particles larger than this size range is controlled by differential sedimentation and turbulent acceleration. Thus, one would normally expect that particle inertia plays a negligible role in coagulation due to turbulent shear and the results given in the preceding sections would be applicable. However, toward the higher end of this size range and for moderately large Kolmogorov shear rates, particle inertia can significantly enhance coagulation. Often the parameter regime of interest is one in which the Stokes number $\mathrm{St}=\Gamma_\eta \tau_v$ is small compared with one, but not so small that particle inertia can be neglected altogether. For example, particles with a mean radius of 5 μm and a standard deviation of the particle size distribution of about 10% in a turbulent flow with $\Gamma_\eta = 630\ \mathrm{s}^{-1}$ would have an ideal coagulation rate due to turbulent shear that is about 3 times larger than that due to differential sedimentation and would have St$=0.2$. The direct-numerical simulations of Reade and Collins[15] indicate that considerable preferential concentration of particles can occur even at mod-

TABLE I. The overall coagulation rate coefficient k_c normalized by $\Gamma_\eta a^3$ and the local interaction parameter β are given for various values of the Stokes number. The Taylor microscale Reynolds number R_λ is 47.1 and $\eta/a=1000$.

St	k_c	β
0.0	8.12	1.00
0.05	9.02	1.04
0.1	12.04	1.11
0.15	20.78	1.17
0.2	49.59	1.26

est values of St. This preferential concentration can be expected to significantly enhance the coagulation rate. This motivates us to build upon Chun's[7] recent theoretical and stochastic simulation study of preferential concentration in the limit $\mathrm{St}\ll 1$ to determine the overall rate of coagulation for particles with small but nonzero Stokes numbers. (See Table I.)

We consider first the ideal coagulation rate of inertial particles in the absence of hydrodynamic and colloidal particle interactions. Chun[7] studied the distribution of inertial *ghost* particles that have no interactions and no volume, so that the particles do not collide. This description of the particle distribution is accurate in a dilute suspension for particle separations $r\gg 2a$. Inertial particles are thrown out of regions of high vorticity and their concentration is slightly enhanced in regions of high strain. This tendency can be quantified by the difference of the mean-square strain and rotation rates following inertial particle trajectories from those following fluid particle trajectories. The results of the theory of Chun for these quantities are listed in Table II for two values of the Taylor-scale Reynolds number R_λ. The deviation of the mean-square rotation and strain rates in the vicinity of inertial particle from the value $\frac{1}{2}\Gamma_\eta$ for fluid particles grown in proportion to St for $\mathrm{St}\ll 1$. However, the magnitude of the decrease in the rotation rate seen by the particles is 10 to 40 times larger than the magnitude of the increase in the strain rate.

At particle separations intermediate between the particle diameter and the Kolmogorov length scale, i.e., $2a\ll r\ll\eta$, the pair distribution function was found to grow as a power law with decreasing radial position[7]

TABLE II. The parameters that characterize the clustering of inertial particles at two Taylor microscale Reynolds number $R_\lambda=47.1$ and 57.3. $\langle\Delta(S^2)\rangle_p$ and $\langle\Delta(R^2)\rangle_p$ represent the deviations of the mean-square strain and rotation rates of the fluid in the vicinity of an inertial particle from those of a fluid particle in the limit $\mathrm{St}\ll 1$. Here, the strain and rotation rates are normalized by the Kolmogorov shear rate. The power law exponent c_1 in the expression [Eq. (6)] for the pair distribution function valid in the limit $\mathrm{St}\ll 1$ is also listed.

	$R_\lambda=47.1$	$R_\lambda=57.3$
$\langle\Delta(S^2)\rangle_p/\mathrm{St}$	0.122	0.045
$\langle\Delta(R^2)\rangle_p/\mathrm{St}$	−1.696	−2.135
c_1/St^2	6.558	7.864

$$g(r)=c_0\left(\frac{\eta}{r}\right)^{c_1}, \tag{22}$$

where the power law exponent c_1 can be obtained from either analytical theory or simulations[7] and the prefactor c_0 can be obtained from DNS.[15] c_0 is typically $O(1)$, while $c_1=O(\mathrm{St}^2)$ as $\mathrm{St}\to 0$. The asymptotic behavior of c_1 obtained from the theory is listed in Table II. Because this power law holds over a large range of length scales from $\eta=O(1\ \mathrm{mm})$ to $2a=O(10\ \mu\mathrm{m})$, the pair distribution function may exceed 1 by a significant amount even when St is quite modest.

These results characterizing the preferential concentration of the inertial particles were obtained for only two values of the Taylor-scale Reynolds number $R_\lambda=47.1$ and 57.3 and we shall consider coagulation at these two values. The theoretical development in Chun provides a relationship between the properties listed in Table II and the Lagrangian statistics of the dissipation and enstrophy. Thus, a better understanding of the Reynolds-number dependence of preferential concentration and its effect on coagulation can be obtained by future DNS studies that determine the R_λ dependence of these basic statistics characterizing an isotropic turbulent flow.

If the only effect of inertia was to enhance the pair probability at intermediate length scales and the local interaction of particles that leads to their ultimate collision and coalescence was independent of inertia, then we could express the coagulation rate constant as the product of the rate coefficient $8.12\Gamma_\eta a^3$ for inertialess particles and the pair probability $c_0(\eta/2a)^{c_1}$ obtained by extrapolating Eq. (22) . We define a parameter β whose deviation from 1 captures the effect of inertia on the local particle–particle collision so that the overall rate coefficient is given by

$$k_c=8.12\Gamma_\eta a^3\beta c_0\left(\frac{\eta}{2a}\right)^{c_1}. \tag{23}$$

The value of β will depend only on the Stokes number that characterizes the importance of particle inertia in the local interaction at separations $r=O(a)$. Thus, β will be independent of $\eta/2a$.

Our simulations describe the relative motion of particle pairs in a stochastically varying linear field when their separation is $r<r_\infty$ where $r_\infty\ll\eta$. Thus, the Kolmogorov length scale does not come directly into the simulation and instead of the power law in Eq. (22), we obtain a power law $g=c_0^{\mathrm{sim}}(r_\infty/2a)^{c_1}$ with the same power law exponent c_1 as in the actual turbulent flow but a different pre-exponential factor c_0^{sim}. The value of c_0^{sim} depends on the details of how particles are introduced at the outer boundary, but it can be easily obtained by performing ghost particle simulations similar to those of Chun.[7] Using this value of c_0^{sim} and the coagulation rate constant k_{sim} obtained from the simulations together, we can obtain β as

$$\beta=\frac{k_{\mathrm{sim}}}{c_0^{\mathrm{sim}}8.12\Gamma_\eta a^3}\left(\frac{2a}{r_\infty}\right)^{c_1}. \tag{24}$$

To confirm that this procedure leads to a value of β that is independent of r_∞, we performed simulations for $R_\lambda=47.1$

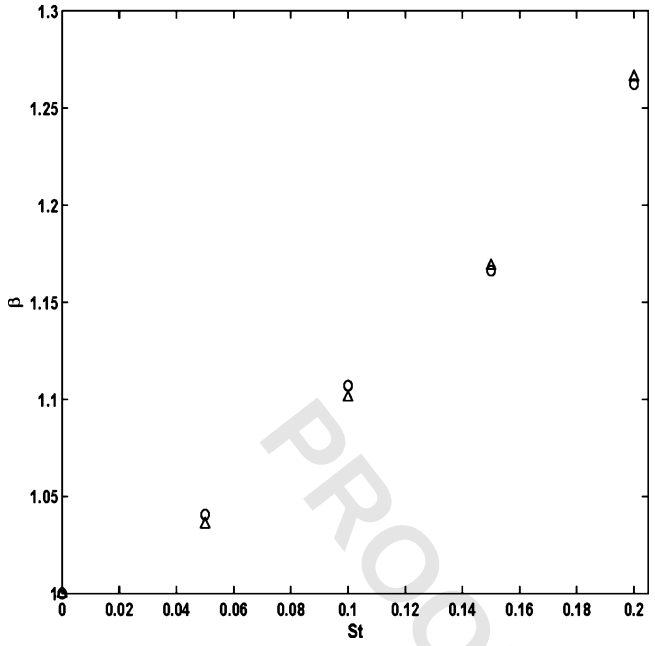

FIG. 5. The factor β describing the effect of particle inertia during the local collision of particle pairs on the rate coefficient is plotted as a function of the Stokes number for two different Taylor-scale Reynolds numbers R_λ =47.1 (circles), R_λ=57.3 (triangles).

and St=0.1 with $r_\infty=5a$, $10a$, $15a$, $20a$ and obtained values of β, 1.10, 1.11, 1.11, 1.10, respectively. These values of the local interaction parameter β show no statistically significant variation with r_∞ despite the fact that the overall rate coefficient k_{sim} increases by 10% as r_∞ is increased from $5a$ to $20a$.

Figure 5 presents results for the parameter β as a function of the Stokes number for R_λ=47.1 (circles) and 57.3 (triangles). The results for the two Taylor-scale Reynolds numbers are nearly identical and the increase in β with St is fit well by

$$\beta = 1 + 0.71\ \text{St} + 2.96\ \text{St}^2. \tag{25}$$

It is interesting to note that the effect of particle inertia on the local coagulation events captured by β is nearly independent of R_λ. The difference between the two simulated values of R_λ is not large, but it is sufficient to produce a significant change in c_1, the degree of preferential concentration, and the overall coagulation rate. Thus, we believe that the absence of any appreciable change in the parameter β describing the local inertial effects is significant. Brunk *et al.*[8] showed that the coagulation rate of inertialess particles is controlled primarily by the straining motion and was weakly dependent on the rotational motion of the fluid. If we assume that the straining motion also is the predominant determinant of β for small but finite St, then the fact (seen in Table II) that the strain rate experienced by the particles is not significantly altered from that of fluid particles may explain the weak dependence of β on R_λ.

For St=0.2, the overall ideal rate coefficient given by Eq. (23) includes an enhancement on the order of 20% due to particle inertia acting during the local particle interactions and a much larger enhancement due to the preferential concentration that accumulates over the range of length scales $2a \ll r \ll \eta$. As an illustration, we present in Table I the coagulation rate normalized by $\Gamma_\eta a^3$ as a function of the Stokes number for $\eta/a=1000$.

Next, we consider simulations of finite Stokes number particles with noncontinuum hydrodynamic interactions and van der Waals attractions. The results of these simulations will be expressed in terms of the collision efficiency α defined as the ratio of the rate coefficient for interacting particles to the ideal rate for inertial particles given by Eq. (23). Since the shear rate and/or particle radius must be relatively large in order to have a finite St, only moderately large values of N_S (the ratio of van der Waals to viscous forces) are relevant to inertial particles. We present results for α as a function of the Stokes number in Fig. 6 for Kn=0.1, N_L =238.8, and N_S=10 (circles) and 100 (squares). It can be

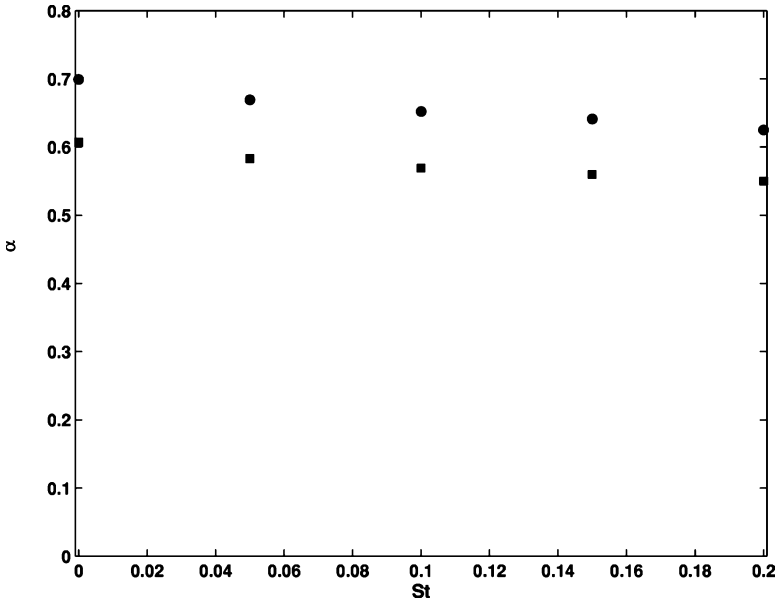

FIG. 6. The collision efficiency α is plotted versus the particle Stokes numbers for N_S=10 (circles) and 100 (squares). The particle radius is 1.9 μm and Kn=0.1.

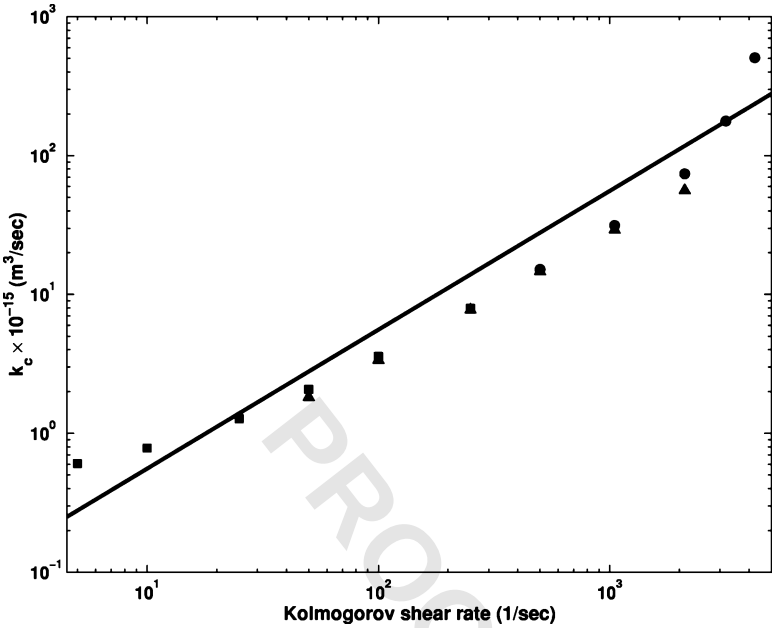

FIG. 7. The coagulation rate coefficient k_c is plotted as a function of the Kolmogorov shear rate for 1.9 μm radius water drops in air with a pressure of 1 atm and a temperature of 300 K. The corresponding nondimensional numbers are Kn=0.035, N_L=238.76 and Pe $=5N_S$. The squares denote the results with Brownian motion but without particle inertia. The triangles denote the results without Brownian motion and particle inertia. The circles denote the results with particle inertia but without Brownian motion. The solid line represents the ideal coagulation rate without particle interactions and inertia, i.e., $k_c=8.12\Gamma_\eta a^3$.

seen that the collision efficiency is nearly independent of the Stokes number. This indicates that for small Stokes numbers, one can approximate the coagulation rate as the product of an ideal rate [Eq. (23)] that takes account of inertial effects and a collision efficiency computed in the absence of inertial effects. At large N_S, two particles must come very close together before van der Waals forces have a significant effect on their relative motion. At such close separations, the strong lubrication interactions make the effects of particle inertia negligible. As a result, one can approximately decouple the effects of particle inertia, which dominate at large particle separations, and the effects of particle interactions, which are important at smaller separations.

VI. CONCLUSIONS

We have conducted stochastic numerical simulations to determine the initial rate of coagulation of monodisperse aerosol particles in a turbulent flow. Particular emphasis was given to the effects of the finite mean-free path of the gas and of particle inertia as these factors, which influence aerosol coagulation, have not been considered in previous studies of the turbulent coagulation of colloidal particles. In addition, we considered the coupled effects of Brownian motion and turbulence on particle coagulation. Although these coupled effects are important in both colloidal and aerosol systems, they have not been examined in previous investigations of turbulent coagulation of colloids. We considered the following three cases: (a) intermediate turbulent shear rates and particle radii for which particle inertia and Brownian motion are negligible; (b) small shear rates and radii for which Brownian motion and turbulent shear both drive particle collisions; and (c) large sizes and shear rates where particle inertia influences the turbulent-shear-driven encounters. In each of these cases, we first examined the ideal rate coagulation for particles in the absence of particle interactions. The ideal rate for mixed Brownian and turbulent shear coagulation was computed as a function of the Peclet number and the ideal rate for inertial particles was determined as a function of the Stokes number and the ratio of the Kolmogorov length to the particle radius, i.e., η/a. Subsequently, we determined the collision efficiency defined as the ratio coagulation rate constant for particles undergoing noncontinuum hydrodynamic interactions and van der Waals attractions to the ideal rate.

In addition to Pe and St, the collision efficiency depends on the parameters N_S and N_L that characterize the importance of van der Waals forces and the Knudsen number Kn that characterizes the importance of noncontinuum effects on the viscous resistance to interparticle motion. In the absence of particle inertia, the only turbulence parameter affecting the coagulation rate is the Kolmogorov shear rate Γ_η. As a result, the St=0 results are independent of the turbulence Reynolds number R_λ. At finite St, the strength of the preferential concentration of particles does depend on R_λ and it has only been evaluated for a limited range of R_λ. However, we have found that the coagulation rate for inertial particles can be determined as the product of the pair probability g of noninteracting particles at $r=2a$, a parameter β that accounts for the effects of inertia during local interactions and the collision efficiency α. We have found that β is only a function of St and is insensitive to R_λ, while α depends only on $N_S, A/kT$, and Kn and is nearly independent of St and R_λ.

The presentation of coagulation rates in nondimensional form elucidates the roles of the many mechanisms that influence aerosol coagulation. However, to give a more practical understanding, it is useful to present the results for the overall dimensional coagulation rate constant. In Fig. 7, we present the dimensional coagulation rate constant for water drops with radii of 1.9 μm in air at 300 K and 1 atmosphere as a function of the Kolmogorov shear rate for $5\ \mathrm{s}^{-1} \leqslant \Gamma_\eta \leqslant 4240\ \mathrm{s}^{-1}$. This range of shear rates yield $1.64 \leqslant \mathrm{Pe} \leqslant 1390$, $0.33 \leqslant N_S \leqslant 277$ and $\mathrm{St} < 0.2$. The Kolmogorov length scale is held fixed at η=1.9 mm. For $100\ \mathrm{s}^{-1} \leqslant \Gamma_\eta \leqslant 1000\ \mathrm{s}^{-1}$, Brownian motion and particle inertia both have a

small effect on the coagulation rate. For this range of shear rates, the coagulation rate is slightly smaller than the ideal coagulation rate for inertialess, non-Brownian particles (indicated by the solid line). The collision efficiency in this range is about 0.55 whereas a typical collision efficiency for a colloidal particle with similar a would be 0.27. For $\Gamma_\eta \leqslant 100\ s^{-1}$, Brownian motion increases the coagulation rate above the value due to turbulent shear alone. At sufficiently small Γ_η, the coagulation rate would approach the value $3.5 \times 10^{-16}\ m^3\ s^{-1}$ for Brownian drops in the absence of flow. At shear rates larger than $1000\ s^{-1}$, the coagulation rate exhibits a rapid increase due to the preferential concentration of particles caused by particle inertia as well as the enhancement of the local collision rate by particle inertia.

Most previous theoretical and experimental studies of turbulent coagulation have focused on particles suspended in liquids. However, these studies cannot be directly used to estimate the coagulation rate of aerosol particles. The coagulation rate constant for aerosol particles typically exceeds that for colloidal particles for the same particle radii a and Kolmogorov shear rate Γ_η. The smaller dynamic viscosity of a gas makes the Peclet number smaller in an aerosol than a comparable colloidal suspension. Particles coagulate more rapidly under the coupled influence of Brownian motion and turbulent shear than they would by turbulent shear acting alone. Since Brownian effects remain important for Pe as high as 20, one may have to go to surprisingly high Kolmogorov shear rates to achieve coagulation characteristic of turbulent shear alone. This was illustrated by the example in Fig. 7. The collision efficiency of aerosols is typically larger than that of colloidal particles. The Hamaker constant for particles interacting through a gas is typically about a factor of 2 larger than that for particles interacting in a liquid. More importantly the smaller dynamic viscosity of a gas leads to a much smaller value of N_S, the ratio of viscous to van der Waals forces, than would occur in a comparable colloidal system. Thus, van der Waals attractions can lead to coagulation of aerosol particles at larger separations and the particle collisions are less severely retarded by lubrication interactions. At high enough shear rates, so that $N_S \to \infty$, the collision efficiency in a colloidal system would approach zero. However, the finite mean-free path of the gas in an aerosol system limits the strength of the lubrication interaction and leads to a finite collision efficiency even in the absence of van der Waals forces. The effect of the finite mean-free path increases with increasing N_S as well as with increasing Kn. For example, the mean free path induces 13% and 63% increases in the collision efficiency at N_S=3.27 and 138.02, respectively, for simulations of the coalescence of water drops at atmospheric pressure without Brownian motion and particle inertia in Fig. 7, compared to the corresponding continuum results. Finally particle inertia leads to an abrupt increase in the coagulation rate of aerosol particles when the particle Stokes number grows to values on the order of 0.1 or larger. This dramatic increase results primarily from the preferential concentration of inertial particles that accrues over a range of length scales from the particle diameter to the Kolmogorov scale.

Turbulence can drive collisions between particles in two ways: through the shearing motion of the gas and through the differences in velocities of polydisperse particles induced by turbulent accelerations. By focusing on turbulent coagulation of monodisperse aerosols in this paper, we have studied coagulation by turbulent shear in isolation from effects of turbulent acceleration. The ideal coagulation rate by turbulent shear scales with a^3, while that due to turbulent acceleration scales with $a^3\delta a$ where a is a characteristic particle radius and δa is the difference of the two particle radii.[4] In practice, turbulent shear can be isolated in ideal laboratory experiments using small $a \approx 1-3\ \mu m$ particles with small initial polydispersity $\delta a/a \approx 10\%$. To determine the coagulation rate of aerosols of larger size and/or greater polydispersity, one should consider the coupled effects of turbulent shear and acceleration. Relatively little is known about the coagulation rate of aerosol particles due to turbulent acceleration, however. Saffman and Turner[4] estimated the ideal turbulent coagulation rate assuming that the effects of shear and acceleration could be superimposed linearly. They also assumed that the turbulent shear and acceleration did not change during a particle interaction. Chun[7] calculated the ideal coagulation rate due to the coupled effects of shear and turbulent acceleration in an evolving turbulent flow. Chun's results indicate the role of preferential concentration on the coagulation rate and show that the two driving forces cannot be superimposed as assumed by Saffman and Turner. Pinsky *et al.*[33] computed the coalescence rate of $10-30\ \mu m$ water drops due to differential sedimentation and turbulent acceleration in a stationary two-dimensional model of turbulence using an approximate treatment of the hydrodynamic interactions. Pinsky *et al.* results are approximate and cover a limited parameter regime, but they demonstrate the importance of turbulence in influencing the coagulation rate under conditions relevant to coalescence of rain drops in clouds. A more complete parametric study of mixed turbulent acceleration and shear coagulation that includes a realistic model of the turbulent flow and complete description of the particle interactions would be desirable to predict aerosol coagulation over a wider range of circumstances.

ACKNOWLEDGMENTS

Financial support for this work was provided by NASA Grant No. NAG3-2349. The direct-numerical simulations for the ideal coagulation rate due to turbulent shear were performed by Aruj Ahluwalia.

[1] H. R. Pruppacher and J. D. Klett, *Microphysics of Clouds and Precipitation* (D. Reidel, Boston, 1978).
[2] J. D. Klett and M. H. Davis, "Theoretical collision efficiencies of cloud droplets at small Reynolds numbers," J. Atmos. Sci. **30**, 107 (1973).
[3] C. L. Lin and S. C. Lee, "Collision efficiency of water drops in the atmosphere," J. Atmos. Sci. **32**, 1412 (1975).
[4] P. G. Saffman and J. Turner, "On the collision of drops in turbulent clouds," J. Fluid Mech. **1**, 16 (1956).
[5] S. Sundaram and L. R. Collins, "Collision statistics in an isotropic, particle-laden turbulent suspension. Part 1. Direct Numerical Simulations," J. Fluid Mech. **335**, 75 (1997).
[6] Y. Zhou, A. S. Wexler, and L. P. Wang, "On the collision rate of small particles in isotropic turbulence. 2. Finite inertia case," Phys. Fluids **10**, 1206 (1998).
[7] J. Chun, "Coagulation of aerosols by Brownian motion and turbulence," Ph.D. dissertation, Cornell University, 2003.

[8]B. K. Brunk, D. L. Koch, and L. W. Lion, "Turbulent coagulation of colloidal particles," J. Fluid Mech. **364**, 81 (1998).
[9]D. L. Koch and S. B. Pope, "Coagulation-induced particle-concentration fluctuations in homogeneous, isotropic turbulence," Phys. Fluids **14**, 2447 (2002).
[10]L. M. Hocking, "The effect of slip on the motion of a sphere close to a wall and of two adjacent spheres," J. Eng. Math. **7**, 207 (1973).
[11]R. H. Davis, "The rate of coagulation of a dilute polydispersed system of sedimenting spheres," J. Fluid Mech. **145**, 179 (1984).
[12]R. R. Sundararajakumar and D. L. Koch, "Non-continuum lubrication flows between particles in a gas," J. Fluid Mech. **313**, 283 (1996).
[13]P. K. Yeung and S. B. Pope, "Lagrangian statistics from direct numerical simulations of isotropic turbulence," J. Fluid Mech. **207**, 531 (1989).
[14]J. Abrahamson, "Collision rates of small particles in vigorously turbulent fluid," Chem. Eng. Sci. **30**, 1371 (1975).
[15]W. C. Reade and L. R. Collins, "Effect of preferential concentration on turbulent collision rates," Phys. Fluids **12**, 2530 (2000).
[16]E. Balkovsky, G. Falkovich, and A. Fouxon, "Intermittent distribution of inertial particles in turbulent flows," Phys. Rev. Lett. **86**, 2790 (2001).
[17]G. Falkovich and A. Pumir, "Intermittent distribution of heavy particles in a turbulent flow," Phys. Fluids **16**, L47 (2004).
[18]G. Falkovich, A. Fouxon, and M. G. Stepanov, "Acceleraton of rain initiation by cloud turbulence," Nature (London) **419**, 151 (2002).
[19]M. Pinsky, M. Shapiro, A. Khain, and H. Wirzberger, "A statistical model of strains in homogeneous and isotropic turbulence," Physica D **191**, 297 (2004).
[20]J. F. Brady and G. Bossis, "Stokesian dynamics," Annu. Rev. Fluid Mech. **20**, 111 (1988).
[21]S. Kim and S. J. Karrila, *Microhydrodynamics: Principles and Selected Applications* (Butterworth-Heinemann, Boston, 1991).
[22]G. K. Batchelor and J. T. Green, "The hydrodynamic interaction of two small freely-moving spheres in a linear flow field," J. Fluid Mech. **56**, 375 (1972).
[23]D. J. Jeffrey and Y. Onishi, "Calculation of the resistence and mobility functions for two unequal rigid spheres in low Reynolds number flow," J. Fluid Mech. **139**, 261 (1984).
[24]W. B. Russel, D. A. Saville, and W. R. Schowalter, *Colloidal Dispersions* (Cambridge University Press, Cambridge, 1989).
[25]J. H. Schenkel and J. A. Kitchener, "At test of the Derjaguin–Verwey–Overbeek theory with a colloidal suspension," Trans. Faraday Soc. **56**, 161 (1960).
[26]G. Bossis and J. F. Brady, "Self-diffusion of Brownian particles in concentrated suspensions under shear," J. Chem. Phys. **87**, 5437 (1987).
[27]L. P. Wang, A. S. Wexler, and Y. Zhou, "On the collision rate of small particles in isotropic turbulence. 1. Zero-inertia case," Phys. Fluids **10**, 266 (1998).
[28]K. D. Squires and J. K. Eaton, "Particle response and turbulence modification in isotropic turbulence," Phys. Fluids A **2**, 1191 (1991).
[29]D. L. Feke and W. R. Schowalter, "The effect of Brownian diffusion on shear-induced coagulation of colloidal dispersions," J. Fluid Mech. **133**, 17 (1983).
[30]A. Z. Zinchenko and R. H. Davis, "Collision rates of spherical drops or particles in a shear-flow at arbitrary Peclet numbers," Phys. Fluids **7**, 2310 (1995).
[31]D. Pnueli, C. Gutfinger, and M. Fichman, "A turbulent-Brownian model for aerosol coagulation," Aerosol Sci. Technol. **14**, 201 (1991).
[32]R. F. Probstein, *Physicochemical Hydrodynamics* (Butterworth, Boston, 1989).
[33]M. Pinsky, A. Khain, and M. Shapiro, "Collisions of small drops in a turbulent flow. Part I: Collision efficiency. Problem formulation and preliminary results," J. Atmos. Sci. **56**, 2585 (1999).